Revision 2

P-V-T equation of state and high-pressure behavior of $CaCO_3$ aragonite

Ying Li[1, 2], Yongtao Zou[1], Ting Chen[3], Xuebing Wang[3], Xintong Qi[3], Haiyan Chen[1], Jianguo Du[2], Baosheng Li[1]

[1] *Mineral Physics Institute, Stony Brook University, Stony Brook, NY 11794-2100, USA*
[2] *CEA Key Laboratory of Earthquake Prediction (Institute of Earthquake Science), China Earthquake Administration, Beijing, 100036, China*
[3] *Department of Geosciences, Stony Brook University, Stony Brook, NY 11794-2100, USA*

Abstract

The equation of state of aragonite was determined by *in situ* synchrotron X-ray diffraction experiments on a hot-pressed polycrystalline specimen of aragonite within its stability field up to 5.8 GPa and 1173 K. As a complement to this experimental study, first principles density functional theory calculations were performed up to 20 GPa at 0 K. Thermoelastic parameters for aragonite ($CaCO_3$) were derived by a least-squares fit of the experimental P-V-T data to the third-order Birch-Murnaghan equation of state (EOS), yielding the bulk modulus and its pressure and temperature derivatives $K_0 = 65.24 \pm 0.24$ GPa, $K_0' = 4.95 \pm 0.12$, $(\partial K_T/\partial_T)_P = -0.024 \pm 0.002$ GPa K^{-1} and volume thermal expansion $\alpha_{300} = (6.1 \pm 0.7)\times10^{-5}$ K^{-1}. The analyses of the axial compressibility at ambient temperature show that the *c*- axis is much more compressible than the *a*- and *b*- axes. Based on first principles calculations, the anisotropic compression behavior of aragonite structure is explained by the heterogeneous shortening of <Ca-O> and <C-O> bond lengths and the rotation of <O-C-O> angles along the *a*-, *b*-, and *c*-axes, whereas the unit cell volume change of aragonite under compression is accommodated by comparable compression rate of the CaO_9 polyhedra and the voids in the crystal lattice. The results attained from this study provide important thermoelastic parameters for understanding the thermodynamic behavior and chemical reactions involving aragonite at subduction zone conditions.

Keywords: Aragonite, X-ray diffraction, equation of state, axial compressibility, high pressure and high temperature, first principles density functional theory calculation

Introduction

Dissolution of carbonates is an important mechanism for transferring carbon into the mantle and ultimately recycling back into the atmosphere to balance the carbon flux (Kerrick and Connolly, 1998; Frezzotti et al., 2011). $CaCO_3$ is a dominant carbon-bearing mineral and exists widely in the crust, mainly in pelagic marine sediments such as clay-rich marls and carbonate ooze (Plank and Langmuir, 1998). When entrained by the subducting process, the polymorphic phases of $CaCO_3$ (e.g., calcite, aragonite and veterite) can be transported to deep depths in the subduction zone (Dasgupta and Hirschmann, 2010; Perchuk and Korepanova, 2011).

In recent years, the high-pressure properties and behaviors of $CaCO_3$ have attracted considerable interest in order to facilitate our understanding of the global carbon cycle by identifying potential carbon storage pathways in the Earth. Of particular interest is aragonite, a phase stable at the P-T conditions corresponding to the lower crust and the uppermost mantle, which has been identified to be a major carbonate phase that can store oxidized carbon in mantle-related assemblages of high-pressure metamorphic rocks (Litasov and Ohtani, 2010; Grassi and Schmidt, 2011). The thermodynamic calculation results of Kerrick and Connolly (2001) have shown that clay-rich marls along low-temperature geotherms at depths of <180km have undergone virtually no devolatilization in subduction zone; aragonite is also a main carbon storage phase in siliceous limestones and carbonate ooze at these depth ranges.

Previously, the behavior of aragonite at high pressures and temperatures has been studied by infrared spectroscopy (Kraft et al., 1991), X-ray diffraction (Martinez et al., 1996; Santillán and

Williams, 2004; Ono et al., 2005), Brillouin scattering (Liu et al., 2005) and Raman spectroscopy (Kraft et al., 1991; Williams et al., 1992; Gillet et al., 1993). At ambient pressure, aragonite spontaneously reverts to calcite at temperatures above 673 K (Carlson and Rosenfeld, 1981); whereas at high pressures, metastable phases of $CaCO_3$, Calcite II and III, have been observed within the stability field of aragonite (Merrill and Bassett, 1975). Calcite III has been considered as a disordered variant of aragonite (Fong and Nicol, 1971). The phase transitions between calcite II, calcite III and aragonite were also identified within the pressure of 0-6 GPa (Suito et al., 2001; Catalli and Williams, 2005; Ono et al., 2005). No phase transitions were observed in aragonite up to 30-40 GPa according to Kraft et al. (1991) and Gillet et al. (1993). At pressures above 40 GPa, it transforms to post-aragonite structure and remains stable at the lower mantle pressures (Ono et al., 2005). To date, the bulk modulus and its pressure derivative are still scattered, ranging from 64 to 88 GPa and 2.3 to 5.3, respectively, High temperature P-V-T equation of state (EOS) of aragonite has only been studied by Martinez et al. (1996) by in situ X-ray powder diffraction experiment at pressures of 3-8 GPa, and the temperature derivative of the bulk modulus was not conclusively constrained due to the ambiguities in the pressure derivative. In this study, using *in situ* synchrotron X-ray diffraction techniques, the *P-V-T* behavior of aragonite was studied up to 6 GPa and 1173 K. In addition, first principles calculations were performed to gain insight into the crystal chemistry and compression mechanisms of aragonite under high pressure.

Experimental procedures and specimen description

A polycrystalline specimen of aragonite was synthesized in a 1000-ton uniaxial split-cylinder apparatus (USCA-1000) at the High Pressure Laboratory of Stony Brook University using reagent-grade calcite powder as starting material. The specimen was hot-pressed at pressure of 8 GPa and

temperature of ~ 700K for 10 hours. Aragonite is quenchable and remains stable after recovery from high pressure and temperature (see also Ono et al., 2005). As evidenced in Fig. 1, the synthesized specimen is a single phase of aragonite. The sample appeared to be well-sintered with a bulk density of 2.92 (1) g/cm^3 as measured by Archimedes immersion method (Wilson, 2012), which is within 0.2-0.4% of the theoretical density from our X-ray diffraction measurement (2.932 (1) g/cm^3) and those (2.926-2.933 g/cm^3) attained by Huggins (1922).

The high-pressure and high-temperature in situ experiments were conducted using a DIA-type cubic-anvil apparatus at the X17B2 beamline of the National Synchrotron Light Source (NSLS) at Brookhaven National Laboratory (BNL). An energy-dispersive X-ray method was employed to collect the diffracted X-rays at a fixed Bragg angle of $2\theta = 6.44^{\circ}$. It is worth noting that using a hot-pressed polycrystalline sample instead of a powder decreases the microscopic deviatoric stress experienced by the individual grains so that the diffraction peaks are less likely to exhibit broadening during compression at room temperature (e.g., Li et al., 1996). Details of the experimental assembly setup used in this study can be found elsewhere (Weidner et al., 1992; Li et al., 2004; Zhang et al., 2013). The pressure-transmitting medium was made of pre-compressed boron epoxy (4:1 wt% ratio) and in cubic shape with an edge length about 6.4 mm. The aragonite specimen was embedded in a NaCl-BN powder mixture (10:1 wt% ratio) inside a cylindrical container of boron nitride. The NaCl powder was also used as an internal pressure standard and the cell pressure was calculated from its equation of state (Decker, 1971). The pressure uncertainties are about 0.2 GPa in the *P-T* range of this study, mainly resulting from the uncertainties of the lattice parameters of NaCl measured at each experimental condition. The temperature was measured by a W/Re25%-W/Re3% thermocouple with the thermal junction placed adjacent to the specimen (e.g.,

Li et al., 2004). The vertical and radial temperature gradients over the entire sample chamber were estimated to be less than 20 K/mm (Weidner et al., 1992; Wang et al., 1998).

The sample was initially compressed to the highest pressure (7.7 GPa) at ambient temperature and then the temperature was increased to a maximum of 1173 K. Subsequently, the experiment was continued via a series of cooling/heating cycles at various ram loads (Fig. 2). To minimize the effect of deviatoric stress generated during compression/decompression at room temperature, high temperature data were only collected along cooling after reaching the peak temperatures. To avoid the occurrence of phase transition and disordered structure (Suito et al., 2001; Ono et al., 2005), we selected 1173, 973, 773, and 300 K as the temperature conditions for data collection in each cycle; from 773 to 300K, the temperature was quickly quenched by switching off the power supply. The lattice parameters were obtained by Le Bail full spectrum fit (Le Bail, 2005) using the software package GSAS (Larson and Von Dreele, 2000) and the EXPGUI (Toby, 2001).

The first principles density-functional theory (DFT) calculations were performed using the Vienna ab initio simulation package (VASP) code (Kresse and Furthmüller, 1996a; 1996b). A plane wave energy cutoff of 700 eV was used for the calculation. The tetrahedron method combined with Blöchl corrections (Blöchl, 1994) has been used for the Brillouin-zone integration over a *k* mesh of 6×4×5 for the orthorhombic aragonite. The combined GGA-PAW (generalized gradient approximation and the projector augmented wave) functionals were used for accurate ab initio calculations on energies and structures. The core region cutoff of the potentials is 3.0 a.u. for calcium, 1.5 a.u. for carbon, and 1.52 a.u. for oxygen. The current parameterization assures a convergence of total energy to better than 1meV/atom, forces to better than 0.01eV/Angstrom, and pressure to less than 0.2 GPa.

Results and discussion

Room-temperature equation of state

Lattice parameters and unit-cell volumes of $CaCO_3$ aragonite attained along various isotherms from 300 to 1173 K at pressures up to 7.7 GPa are listed in Table 1. X-ray diffraction spectra obtained at ambient (before and after the experiment) and the peak P-T conditions are compared in Fig. 1. The diffraction peaks were indexed by the orthorhombic unit cell of aragonite with *Pmcn* space group. Within the resolution of the present X-ray diffraction data, no structural changes were observed up to the peak P-T conditions of the current experiment. The unit-cell volume at ambient condition (V_0) was measured to be 226.71 ± 0.01 Å^3, which is in good agreement with the values of 226.7 ± 0.3 Å^3 and 226.96 ± 0.01 Å^3 reported by Santillán and Williams (2004) and Parker et al. (2010), respectively. The current result is ~0.2 % smaller than the values of 227.14 Å^3 and 227.2 ± 0.1 Å^3 reported by Martinez et al. (1996) and Ono et al. (2005), respectively, which could be due to variations of the chemical composition in the samples used in different studies.

The *P-V* data attained at 300 K were fitted by using the third-order Birch-Murnaghan EOS, as shown below,

$$P(V,T) = \frac{3}{2} K_0 \left[\left(\frac{V_0}{V} \right)^{\frac{7}{3}} - \left(\frac{V_0}{V} \right)^{\frac{5}{3}} \right] \times \left\{ 1 + \frac{3}{4} \left(K_0' - 4 \right) \left[\left(\frac{V_0}{V} \right)^{\frac{2}{3}} - 1 \right] \right\} \qquad (1)$$

where K_0, K_0', and V_0 are the isothermal bulk modulus, the pressure derivative of the isothermal bulk modulus, and the unit-cell volume at ambient conditions, respectively. A least squares fit of the present room T data to Eq. 1 with all parameters free yields V_0 = 226.72 ± 0.01 Å^3, K_0 = 65.24 ± 0.24 GPa and K_0' = 4.95 ± 0.12, which are in good agreement with those of Ono et al. (2005) (V_0 = 227.2 ± 1.0 Å^3, K_0 = 67.1 ± 6.3 GPa and K_0' = 4.7 ± 0.8) (see also Fig. 3). The bulk modulus value

compares well with the result of 65.4 ± 0.5 GPa from high *P-T* X-ray study by Martinez et al. (1996), 67.1 ± 6.3 GPa by Ono et al. (2005), and 66.66 GPa reported by Salje and Viswanathan (1976). If we fix K_0' to 4.0, fitting of Eq. 1 gives a result of V_0 = 226.7 ± 2.0 Å^3, K_0 = 66.88 ± 0.05 GPa, which is in agreement within mutual uncertainties with the K_0 value of 64.5 GPa and 64.81 ± 3.48 GPa reported by Martens et al. (1982) and Martinez et al. (1996), respectively. The K_0 value from this study is also in good agreement with the adiabatic bulk modulus K_{S0} = 68.9 ± 1.4 GPa (corresponding K_0 ~ 67.4 GPa) derived by Brillouin spectroscopy (Liu et al., 2005), and in reasonable agreement with 69.6 GPa and 71 GPa attained by previous theoretical calculations (Pavese et al., 1992; Fisler et al., 2000). As shown in Fig. 3, the trend of the compression curve from the current experimental study agrees well with that predicted by our first principles calculations despite there being a ~2.5% difference in the absolute values of volume caused by the well-known underbinding of GGA. By comparison, Santillán and Williams (2004) reported a value of K_0 = 88 GPa (with K_0' = 4), which is significantly higher than those from the other studies (see Table 2). A closer examination of Fig. 3 indicates that the high bulk modulus of Santillán and Williams (2004) most likely results from the scatter in the unit cell volumes, especially those at pressure above 15 GPa, presumably caused by deviatoric stress after the solidification of the methanol-ethanol-water pressure medium.

High-temperature equation of state

The *P-V-T* relations of aragonite were investigated at pressures and temperatures up to ~6 GPa and 1173 K by fitting the attained experimental data from present study to the high-temperature Birch-Murnaghan (HTBM) equation of state (Eq. 1). The pressure derivative K_0' is assumed to be constant in Eq. 1 throughout the whole temperature range. The temperature dependence of the bulk

164 modulus is expressed by a linear function of temperature (Eq. 2), assuming that the temperature
165 derivative is constant throughout the temperature range of present study.
166
167 $$K_T = K_0 + (\partial K_T/\partial T)_P (T - 300) \quad (2)$$
168 $$K_T' = K_0' \quad (3)$$
169 The unit-cell volume V_T at zero-pressure and a given temperature T, is expressed as
170 $$V_T = V_0 \exp \int_{300}^{T} \alpha_T dT \quad (4)$$
171 $$\alpha_T = a_0 + a_1 T \quad (5)$$
172 where V_0 is the unit-cell volume at ambient conditions, α_T is the volume thermal expansion at
173 ambient pressure and a given temperature T, a_0 and a_1 are constant parameters. Table 2 lists the
174 values of V_0, K_0, K_0', $(\partial K_T/\partial T)_P$, a_0 and a_1 derived by fitting our data (Table 1) to Eqs. 1-5. We
175 observe that when none of the parameters is constrained, the uncertainties in the derived parameters
176 are large (Table 2), which might be due to the large number of free parameters relative to the total
177 experimental data points; this observation remains true even though the fitting results (K_0 = 64.5 ±
178 4.2 GPa and K_0' = 5.3 ± 2.3) are in general agreement with those from room temperature data alone.
179 Alternatively, when K_0 and K_0' were fixed to 65.24 GPa and 4.95, respectively, as those derived at
180 room-temperature, and the following results were obtained: V_0 = 226.7 ± 0.1 Å^3, $(\partial K_T/\partial T)_P$ = -0.024
181 ± 0.002 GPa K^{-1} and α_{300} = (6.1 ± 0.7)×10^{-5} K^{-1}. Note that the results of $(\partial K_T/\partial T)_P$ and the thermal
182 expansion coefficients from the constrained fit are nearly identical to those from unconstrained fit,
183 but with much smaller uncertainties. It should be pointed out that the apparent difference between
184 $(\partial K_T/\partial T)_P$ = -0.024 ± 0.002 GPa K^{-1} attained in present study and that of -0.018 ± 0.002 GPa K^{-1}
185 reported by Martinez et al. (1996) is believed to be caused by the difference in K_{T0}' used in the

respective fits; for instance, if the values of K_0 and K_0' were fixed to those from Martinez et al. (1996), the same value of $(\partial K_T/\partial T)_P$ = -0.018 ± 0.002 GPa K^{-1} was obtained (see Table 2). In addition, the resultant thermal expansion coefficient α_{300} is in excellent agreement with that from Martinez et al. (1996). Figure 4 shows the measured unit cell volumes and the isothermal compression curves derived from this study superimposed with those of Martinez et al. (1996), the good agreement between the two datasets can be clearly seen, except for the data at ~7.5 GPa and 1173 K.

Crystal structure of aragonite under compression

A linear fit to the a/a_0, b/b_0 and c/c_0 results versus pressure yielded the linear compressibility of aragonite at room temperature (Table 3) of $(2.6 \pm 0.2)\times10^{-3}$ GPa^{-1}, $(4.8 \pm 0.4)\times10^{-3}$ GPa^{-1} and $(5.9 \pm 0.3)\times10^{-3}$ GPa^{-1} for *a*-, *b*- and *c*-axis, respectively, indicating a strong anisotropy in compression behavior, with the *c*-axis much more compressible than the *a*- and *b*-axis. These results are in excellent agreement with those reported by Martinez et al. (1996) (2.4 ± 0.2, 4.2 ± 0.2 and $5.8 \pm 0.2\times10^{-3}$ GPa^{-1} for *a*-, *b*- and *c*-axis, respectively), and comparable to the results of Fisler et al. (2000) and Liu et al. (2005) (see Table 3).

The crystal structure of aragonite under pressure was further investigated by first principles calculations for the orthorhombic crystal structure (space group *Pmcn*). As shown in Fig. 5, the aragonite structure is characterized by layers of nine-coordinated Ca^{2+} cations, and slightly aplanar CO_3^{2-} groups stacked perpendicular to the *c*- axis (Bragg, 1924; Wyckoff, 1925). With increasing pressure, the bond lengths of <Ca-O> and <C-O> decrease continuously (Table 4 and Fig. 6a); at 20 GPa, the average <Ca-O> bond length has decreased by 6.24%, in comparison, the <C-O> distance has decreased by only ~1%, consistent with previous observations that the CO_3^{2-} groups are rigid units in the aragonite structure (Antao and Hassan et al., 2010; Ye et al., 2012). As a result, in the *b*-

209 *c* plane (Fig. 5), the <Ca-O> bonds experience significant compression with increasing pressure
210 while the <C-O1> bonds along *b*-axis exhibit nearly no compression with a shortening of only
211 0.85% (Fig. 6a). In the *a*-*b* plane, the <Ca-O2> bonds in the direction of *b*-axis show slightly more
212 shortening (6.42-6.68%) than that of the <Ca-O1> bonds (6.06%) along the *a*-axis. These
213 anisotropic bond length shortening could account partially for the anisotropic compression behavior
214 of *a*-, *b*- and *c*- axis in aragonite.

215 The unit cell of aragonite can be considered as consisting of the four CaO9 polyhedra, four
216 aplanar CO_3^{2-} groups, and the voids among polyhedra. Along with the compression of the unit cell
217 of aragonite, the volume of the CaO_9 polyhedra decreases at a slightly lower rate than the voids (Fig.
218 6c); by comparison, the CO_3^{2-} polyhedral undergoes no volume decrease during the compression.
219 Thus, CO_3^{2-} polyhedra have little or no contribution to the volume changes. Moreover, the aplanar
220 characteristics of the CO_3^{2-} groups in the aragonite lattice remain nearly unchanged during
221 compression except for the slight changes in the <O-C-O> angles within the CO_3^{2-} group; this is in
222 good agreement with the small distortion of CO_3^{2-} groups as indicated by the internal vibrational
223 modes under compression (Kraft et al., 1991). As shown in Fig. 6b, from ambient pressure to 20
224 GPa, the <O1-C-O2> angle increases from 120.260° to 120.497°, while the <O2-C-O2> angles
225 decrease from 119.338° to 118.816°, resulting in an increase in the difference between <O1-C-O2>
226 and <O2-C-O2> from 0.9° to 1.7°. This trend is consistent with the increase from 0.7° to 4.5($\pm$1.2)°
227 within 0 - 40 GPa inferred from vibrational spectroscopy data by Kraft et al. (1991). Previously,
228 Holl et al. (2000) carried out a single-crystal X-ray diffraction study on witherite ($BaCO_3$), an
229 isostructural phase of aragonite, up to 8 GPa at ambient temperature. Compared to aragonite,
230 witherite has a slightly different anisotropic compression behavior with $\beta_c > \beta_a = \beta_b$ in the axial
231 compressibility; the pressure dependence of the bond angles <O1-C-O2> and <O2-C-O2>, however,

exhibit the same trend as that of $CaCO_3$ aragonite during compression, suggesting that the same compression mechanisms might be operative in the isostructural carbonate mineral groups.

Implications

In this study, high pressure and temperature data for the equation of state and compressibility of aragonite were obtained by in situ X-ray diffraction at pressures up to 5.8 GPa and temperatures up to 1173 K. Thermoelastic parameters of aragonite ($CaCO_3$) were derived by a least-squares fit of the experimental P-V-T data to the third-order Birch-Murnaghan equation of state, yielding K_{T0} = 65.24 ± 0.24 GPa, K'_{T0} = 4.95 ± 0.12, $(\partial K_T/\partial_T)_P$ = -0.024 ± 0.002 GPa K^{-1} and α_{300}= (6.1 ± 0.7)×10^{-5} K^{-1}. The *c*-axis of aragonite is much more compressible than *a*-axis and *b*-axis, which is related to the anisotropic shortening of <Ca-O> and <C-O> bonds along the *a*-, *b*-, and *c*- axes in the unit cell. The compression of the unit cell of aragonite is mostly the result of the compression of the CaO_9 polyhedra and the voids in the structure, while the CO_3^{2-} groups in the aragonite structure remains aplanar with the <O1-C-O2> angle increasing and the <O2-C-O2> angle decreasing respectively with elevated pressure. The results attained from this study are useful to attain and evaluate the thermoelastic and thermodynamic parameters of aragonite such as the temperature derivative of bulk modulus, density, Grüneisen parameter and its volume dependence at high pressure and high temperature. By comparing the density data of aragonite with other volatile-containing phases in the subduction zone, such as superhydrous phase B or phase D (Litasov et al., 2007; 2008), the effect of the presence of aragonite on the buoyancy of the subducting slabs in the deep mantle can be well estimated. For instance, according to the current P-V relation, the density of aragonite at 12 GPa and 1173 K is about 0.2 g/cm^3 lower than that of superhydrous phase B (Litasov et al., 2007), leading the existence of aragonite more effective for buoyance of the subduction slabs in the deep mantle, compared to H_2O containing phases. In addition, using the method of minimizing the Gibbs

255 free energy, the EOS parameters attained presently are useful for the thermodynamic calculations
256 on the stability field and decarbonation reactions associated with CO_2 degassing and $CaCO_3$
257 dissolution at great depths in the mantle: $CaCO_3$ = CaO (lime) + CO_2 (fluid), $CaCO_3$ + SiO_2 =
258 $CaSiO_3$ (wollastonite) + CO_2 (fluid) and 4 $CaCO_3$ + 4 SiO_2 + $(Mg, Fe)_3Al_2Si_3O_{12}$ (garnet) = 3
259 $Ca(Mg, Fe)Si_2O_6$ (clinopyroxene) + $CaAl_2SiO_6$ (Tschermack's molecule)+ 4 CO_2 (fluid)
260 (Hammouda, 2003). The result will be helpful for the estimation of carbonates amount and the CO_2
261 release in the subduction zone conditions.
262

263 **Acknowledgments**

264 This work is financially supported by the Natural Science Foundation of China (Grant No.
265 41273073), DOE/NNSA (DE-NA0001815), National Science Foundation (EAR1045630) and the
266 Basic Research Project of Institute of Earthquake Science, CEA (02132407). The authors are
267 thankful to Robert C. Liebermann for his valuable suggestions to improve the maunuscript. We also
268 thank the editor Katherine Crispin and Dr. Jianzhong Zhang for their valuable review to improve
269 this manuscript. Use of the X17B2 beamline was supported by COMPRES, the Consortium for
270 Materials Properties Research in Earth Sciences under NSF (EAR 10-43050). Mineral Physics
271 Institute Publication No. 505.
272
273
274 **References cited**

275 Antao, S.M., and Hassan, I. (2010) Temperature dependence of the structural parameters in the
276 transformation of aragonite to calcite, as determined from in situ synchrotron powder X-
277 ray-diffraction data. Canadian Mineralogist, 48, 1225-1236.
278 Blöchl, P.E. (1994) Projector augmented-wave method. Physical Review B, 50, 17953-17978.

279 Bridgman, P.W. (1938) The high pressure behavior of miscellaneous minerals. American Journal
280 of Science, 237, 7-18.
281 Bragg, W.L. (1924) The structure of aragonite. Proceedings of the Royal Society A, 105, 16-39.
282 Carlson, W.D., and Rosenfeld, J.L. (1981) Optical determination of topotactic aragonite-calcite
283 growth kinetics: metamorphic implications. Journal of Geology, 89, 615-638.
284 Catalli, K., and Williams, Q. (2005) A high-pressure phase transition of calcite-III. American
285 Mineralogist, 90, 1679-1682.
286 Dasgupta, R., and Hirschmann, M.M. (2010) The deep carbon cycle and melting in Earth's
287 interior. Earth and Planetary Science Letters, 298, 1-13.
288 Decker, D.L. (1971) High-pressure equation of state for NaCl, KCl, and CsCl. Journal of
289 Applied Physics, 42, 3239-3244.
290 Fisler, D.K., Gale, J.D., and Cygan, R.T. (2000) A shell model for the simulation of
291 rhombohedral carbonate minerals and their point defects. American Mineralogist, 85,
292 217-224.
293 Fong, M.Y., and Nicol, M. (1971) Raman spectrum of calcium carbonate at high pressures.
294 Journal of Chemical Physics, 53, 579-585.
295 Frezzotti, M.L., Selverstone, J., Sharp, Z.D., and Compagnoni, R. (2011) Carbonate dissolution
296 during subduction revealed by diamond-bearing rocks from the Alps. Nature Geoscience,
297 4, 703-706.
298 Grassi, D., Schmidt, and M.W. (2011) The melting of carbonated pelites from 70 to 700 km
299 Depth. Journal of Petrology, 52, 765-789.

Gillet, P., Biellmann, C., Reynard, B., and McMillan, P. (1993) Raman-spectroscopic studies of carbonates Part I: High-pressure and high-temperature behavior of calcite, magnesite, dolomite and aragonite. Physics and Chemistry of Minerals, 20, 1-18.

Hammouda, T. (2003) High-pressure melting of carbonated eclogite and experimental constraints on carbon recycling and storage in the mantle. Earth and Planeraty Science Letters, 214, 357-368.

Hess, N.J., Ghose, S., and Exarhos, G.J. (1991) Raman spectroscopy at simultaneous high pressure and temperature: phase relations of $CaCO_3$ and the lattice dynamics of the calcite $CaCO_3$(II) phase transition. In A.K. Singh, Ed., Recent Trends in High Pressure Research; Proc. X IIIth AIRAPT International Conference on High Pressure Science and Technology, 236-241. Oxford & IBH Publishing Co. Pvt, Ltd., New Delhi.

Holl, C.M., Smyth, J.R., Laustsen, H.M.S., Jacobsen, S.D., and Downs, R.T. (2000) Compression of witherite to 8 GPa and the crystal structure of $BaCO_3$II. Physics Chemistry Minerals, 27, 467-473.

Huggins, M.L. (1922) The crystal structures of aragonite ($CaCO_3$) and related minerals. Physical Review, 19, 354-362.

Kerrick, D.M., and Connolly, J.A.D. (1998). Subduction of ophicarbonates and recycling of CO_2 and H_2O. Geology, 26, 375-378.

Kerrick, D.M., and Connolly, J.A.D. (2001) Metamorphic devolatilization of subducted oceanic metabasalts: implications for seismicity, arc magmatism and volatile recycling. Earth and Planetary Science Letters, 189, 19-29.

Kraft, S., Knittle, E., and Williams, Q. (1991) Carbonate stability in the Earth's mantle: A vibrational spectroscopy study of aragonite and dolomite at high pressures and temperatures. Journal of Geophysical Research, 96, 17997-18009.

Kresse, G., and Furthmüller, J. (1996a) Efficiency of ab-initio total energy calculations for metals and semiconductors using a plane-wave basis set. Computational Materials Science, 6, 15-50.

Kresse, G., and Furthmüller, J. (1996b) Efficient iterative schemes for ab initio total-energy calculations using a plane-wave basis set. Physical Review B, 54, 11169-11186.

Larson, A.C., and Von Dreele, R.B. (2000) General Structure Analysis System (GSAS). Los Alamos National Laboratory Report LAUR. 86-748.

Le Bail, A. (2005) Whole powder pattern decomposition methods and applications-A retrospection. Powder Diffraction, 20, 316-326.

Li, B., Kung, J., and Liebermann, R.C. (2004) Modem techniques in measuring elasticity of earth materials at high pressure and high temperature using ultrasonic interferometry in conjunction with synchrotron X-radiation in multi-anvil apparatus. Physics of the Earth and Planetary Interiors, 143, 559-574.

Li, B., Rigden, S., and Liebermann, R.C. (1996) Elasticity of stishovite at high pressure. Physics of the Earth and Planetary Interiors, 96, 113-127.

Litasov, K., and Ohtani, E. (2010) The solidus of carbonated eclogite in the system CaO-Al_2O_3-MgO-SiO_2-Na_2O-CO_2 to 32 GPa and carbonatite liquid in the deep mantle. Earth and Planetary Science Letters, 295, 115-126.

342 Litasov, K.D., Ohtani, E., Ghosh, S., Suzuki, A., and Funakoshi, K. (2007) Thermal equation of
343 state of superhydrous phase B to 27GPa and 1373 K. Physics of the Earth and Planetary
344 Interiors, 164, 142-160.
345 Litasov, K.D., Ohtani, E., Nishihara, Y., Suzuki, A., and Funakoshi, K. (2008) Thermal equation
346 of state of Al- and Fe-bearing phase D. Journal of Geophysical Research B, 113,
347 DOI: 10.1029/2007JB004937.
348 Liu, L.G., Chen, C.C., Lin, C.C., and Yang, Y.J. (2005) Elasticity of single-crystle aragonite by
349 Brillouin spectroscopy. Physics and Chemistry of Minerals, 32, 97-102.
350 Martens, R., Rosenbauer, M., and Von Gehlen, K. (1982) Compressibilities of carbonates. In W.
351 Schreyer, Ed., High pressure researches in geosciences, p.235-238. Schweizerbartsche
352 Verlagsbuchhandlung, Stuttgart, Germany.
353 Martinez, I., Zhang, J.Z., and Reeder, R.J. (1996) In situ X-ray diffraction of aragonite and
354 dolomite at high pressure and high temperature: Evidence for dolomite breakdown to
355 aragonite and magnesite. American Mineralogist, 81, 611-624.
356 Merrill, L., and Bassett, W.A. (1975) The crystal structure of $CaCO_3$(II), a high-pressure
357 metastable phase of calcium carbonate. Acta Crystallogrphica section B, 31, 343-349.
358 Ono, S., Kikegawa, T., Ohishi, Y., and Tsuchiya, J. (2005) Post-aragonite phase transformation
359 in $CaCO_3$ at 40 GPa. American Mineralogist, 90, 667-671.
360 Pavese, A., Catti, M., Price, G.D., and Jackson, R.A. (1992) Interatomic potentials for the $CaCO_3$
361 polymorphs (calcite and aragonite) fitted to elastic and vibrational data. Physics and
362 Chemistry of Minerals, 19, 80–87.

Parker, J.E., Thompson, S.P., Lennie, A.R., Potter, J., and Tang, C.C. (2010) A study of the aragonite-calcite transformation using Raman spectroscopy, synchrotron powder diffraction and scanning electron microscopy. CrystEngComm, 12, 1590-1599.

Perchuk, A.L., and Korepanova, O.S. (2011) The problem of CO_2 recycling in subduction zones. Moscow University Geology Bulletin, 66, 250-260.

Plank, T., and Langmuir, C.H. (1998) The chemical composition of subducting sediment and its consequences for the crust and mantle. Chemical Geology, 145, 325-394.

Salje, E., and Viswanathan, K. (1976) Phase-diagram calcite-aragonite as derived from crystallographic properties. Contributions to Mineralogy and Petrology, 55, 55–67.

Santillán, J., and Williams, Q. (2004) A high pressure X-ray diffraction study of aragonite and the post-aragonite phase transition in $CaCO_3$. American Mineralogist, 89, 1348-1352.

Suito, K., Namba, J., Horikawa, T., Taniguchi, Y., Sakurai, N., Kobayashi, M., Onodera, A., Shimomura, O., and Kikegawa, T. (2001) Phase relations of $CaCO_3$ at high pressure and high temperature. American Mineralogist, 86, 997-1002.

Toby, B.H. (2001) EXPGUI, a graphical user interface for GSAS. Journal of Applied Crystallography, 34, 210-213.

Wang, Y., Weidne, D.J., and Meng, Y. (1998) Advances in equation of state measurements in SAM-85. In: Manghnani MH, Yagi T (eds) Properties of earth, planetary materials at high pressure, temperature. American Geophysical Union, Washington, DC, pp 365-372.

Weidner, D.J., Vaughan, M.T., Ko, J., Wang, Y., Liu, X., Yeganeh-Haeri, A., Pacalo, R.E., and Zhao, Y. (1992) Characterization of stress, pressure and temperature in SAM85, a DIA type high pressure apparatus, In: Syonov Y, Manghnani MH, (eds), High-pressure research: application to earth and planetary sciences, Geophysical monograph 67, Terra

Scientific Publishing Company and Am. Geophys. Union, Tokyo and Washington, DC, p. 13-17.

Williams, Q., Collerson, B., and Knittle, E. (1992). Vibrational spectra of magnesite ($MgCO_3$) and calcite-III at high pressures. American Mineralogist, 77, 1158-1165.

Wilson, R.M. (2012). Archimedes's principle gets updated. Physics Today, 65(9), DOI: 10.1063/PT.3.1701.

Wyckoff, R.W.G. (1925) Orthorhombic space group criteria and their applications to aragonite. American Journal Science, 209, 145-175.

Ye, Y., Smyth, J.R., and Boni, P. (2012) Crystal structure and thermal expansion of aragonite-group carbonates by single-crystal X-ray diffraction. American Mineralogist, 97, 707-712.

Zhang, J., Zhu, J., Velisavljevic, N., Wang, L., and Zhao, Y. (2013) Thermal equation of state and thermodynamic Grüneisen parameter of beryllium metal. Journal of Applied Physics, 114, 173509.

Figure captions

Figure 1. Selected X-Ray diffraction patterns of aragonite.

Figure 2. Experimental P-T conditions. Phase diagram of aragonite after Suito et al. (2001). Grey long dashed lines represent the P-T path to approach the peak conditions. Bold black lines represent the cycles under different loading pressures. Black short dashed lines represent the phase boundaries between calcite I, calcite II and III. Solid lines represent the phase boundaries between calcite III, aragonite and disordered aragonite. Br = After Bridgman (1938), H.G.&E = After Hess et al. (1991), S.N.&H = After Suito et al. (2001).

Figure 3. P-V relations of aragonite at 300 K obtained in this study, in comparison with previous studies. Solid black curve represents the result of fitting the data of this study yielding $V_0 = 226.72 \pm 0.01$ Å^3, $K_0 = 65.24 \pm 0.24$ GPa and $K_0' = 4.95 \pm 0.12$. Cold compression data were included for comparison but not used in the fit.

Figure 4. *P-V-T* relations of aragonite obtained in this study. Isothermal compression curves at various temperatures are calculated by using the thermoelastic parameters attained in the present study ($V_0 = 226.7 \pm 0.1$ Å^3, $K_0 = 65.24$ GPa, $K_0' = 4.95$, $\partial(K_T/\partial T)_P = -0.024 \pm 0.002$ GPa K^{-1} and $\alpha_{300} = (6.1 \pm 0.7) \times 10^{-5}$ K^{-1}). The errors of unit-cell volumes are less than the size of symbols.

Figure 5. Crystal structure of aragonite $CaCO_3$. The numbers label the <Ca-O> bonds listed out in Table 4.

Figure 6. Variations of the bond lengths (a), angles (b), and volumes of CaO9 polyhedra and voids (c) of aragonite with pressure.

435 **Table 1** Experimental *P-T* conditions, lattice parameters and unit-cell volumes of aragonite obtained by *in-*

436 *situ* X-ray diffraction. Numbers in the parenthesis represent 1σ errors.

T (K)	*P* (GPa)	a (Å)	b (Å)	c (Å)	*V* (Å^3)
Compression before heating					
300	0.00	4.9592(2)	7.9653(2)	5.7392(2)	226.71(1)
300	1.16	4.9485(3)	7.9293(4)	5.6991(3)	223.63(2)
300	3.35	4.9153(4)	7.8563(6)	5.6314(4)	217.46(2)
300	5.13	4.8928(5)	7.8040(7)	5.5749(4)	212.87(2)
300	6.56	4.8797(5)	7.7682(9)	5.5442(5)	210.16(2)
300	7.70	4.8643(6)	7.7418(10)	5.5152(5)	207.70(3)
Compression after heating					
1173	4.55	4.9380(5)	7.9060(6)	5.7638(5)	225.09(2)
1173	5.37	4.9308(4)	7.8818(6)	5.7326(5)	222.79(2)
1173	5.78	4.9211(5)	7.8426(8)	5.7335(3)	221.28(2)
973	2.55	4.9552(5)	7.9772(6)	5.7890(4)	228.83(2)
973	3.38	4.9546(3)	7.9219(8)	5.7552(6)	225.89(2)
973	3.76	4.9422(4)	7.9152(6)	5.7358(6)	224.38(2)
973	4.78	4.9394(4)	7.8722(6)	5.6888(3)	221.21(2)
973	5.29	4.9286(2)	7.8506(3)	5.6777(2)	219.69(1)
773	2.00	4.9532(4)	7.9547(5)	5.7634(3)	227.08(2)
773	2.82	4.9445(3)	7.9222(7)	5.7332(5)	224.58(2)
773	3.26	4.9415(3)	7.8976(6)	5.7090(5)	222.80(2)
773	4.23	4.9272(3)	7.8644(3)	5.6689(3)	219.67(1)
773	4.82	4.9170(3)	7.8467(4)	5.6564(3)	218.24(1)
300	0.00	4.9468(3)	7.9537(4)	5.7393(3)	225.82(2)
300	0.90	4.9454(4)	7.9107(7)	5.7172(4)	223.67(2)
300	1.65	4.9305(4)	7.8930(5)	5.6949(4)	221.62(2)
300	2.18	4.9249(7)	7.8601(8)	5.6694(6)	219.47(2)
300	3.13	4.9194(4)	7.8393(4)	5.6369(5)	217.39(2)
300	3.63	4.9098(4)	7.8204(5)	5.6189(4)	215.75(2)

437

438

439

440 **Table 2** Thermoelastic parameters for aragonite derived from the Birch– Murnaghan (BM) and High

441 Temperature Birch–Murnaghan (HTBM) EOS. Numbers in bracket are errors of the least-squares fitting.

V_0 (Å^3)	K_0 (GPa)	K'_0	$(\partial K_T/\partial T)_P$ (GPa K^{-1})	α_{300} (10^{-5} K^{-1})	a_0 (10^{-5} K^{-1})	a_1 (10^{-8} K^{-2})	References
226.8 (2)	64.5 (42)	5.3 (23)	-0.025 (7)	6.1(14)	4.2 (7)	6.6 (22)	This study
226.7 (1)	65.24*	4.95*	-0.024 (2)	6.1(7)	4.2 (4)	6.4 (10)	
226.9 (1)	64.8*	4*	-0.018 (2)	6.2(7)	4.7 (4)	4.9 (10)	
	64.8 (43)	4*	-0.018 (2)	6.5(1)	6.5 (5)	0.3 (3)	Martinez et al., 1996
	65.4(5)	2.7 (7)	-0.013 (2)	6.7(5)			
	66.66			6.1			Salje and Viswanathan, 1976
	73.1(22)	4*					Ono et al., 2005
	67.1(63)	4.7 (8)					
	88	4					Santillán and Williams, 2004

442 *Values were fixed during data fitting

443

444

Table 3 The linear compressibility of *a*-, *b*- and *c*-axis for aragonite

Linear compressibility	This study	Martinez et al., 1996	Fisler et al., 2000	Liu et al., 2005
	$\times 10^{-3}$ GPa^{-1}	$\times 10^{-3}$ GPa^{-1}	$\times 10^{-3}$ GPa^{-1}	$\times 10^{-3}$ GPa^{-1}
β_a	2.6 ± 0.2	2.4 ± 0.2	2.1	3.0 ± 0.2
β_b	4.8 ± 0.4	4.2 ± 0.2	4.2	4.6 ± 0.2
β_c	5.9 ± 0.3	5.8 ± 0.2	5.8	7.3 ± 0.6

Table 4 Variation of bond lengths (Å), angles (°), polyhedra and voids (Å^3) of aragonite at high pressures calculated by DFT (Density Functional Theory) method

Bond & Angle		(A-B)/A×100%	A-0 GPa	3 GPa	5 GPa	8 GPa	12 GPa	16 GPa	B-20 GPa
Ca-O1 $^{(5)}$	×1	5.07	2.425	2.398	2.387	2.363	2.340	2.319	2.302
Ca-O1 $^{(1)}$	×2	6.06	2.691	2.656	2.635	2.608	2.581	2.553	2.528
Ca-O2 $^{(2)}$	×2	6.42	2.571	2.538	2.516	2.488	2.456	2.429	2.406
Ca-O2 $^{(4)}$	×2	6.38	2.475	2.437	2.417	2.391	2.362	2.338	2.317
Ca-O2 $^{(3)}$	×2	6.68	2.546	2.507	2.482	2.456	2.423	2.398	2.376
<Ca-O>[9]		6.24	2.555	2.519	2.499	2.472	2.443	2.417	2.395
C-O1	×1	0.85	1.292	1.290	1.289	1.287	1.285	1.282	1.281
C-O2	×2	1.08	1.302	1.300	1.298	1.296	1.293	1.290	1.288
<C-O>[3]		1.00	1.299	1.297	1.295	1.293	1.290	1.287	1.286
O1-C-O2	×2	-0.20	120.260	120.296	120.349	120.379	120.458	120.490	120.497
O2-C-O2	×1	0.44	119.338	119.256	119.147	119.078	118.910	118.836	118.816
CaO9 dodecahedron	×4	16.82	30.6977	29.5057	28.8481	27.9724	27.0207	26.2203	25.5338
CO3 tetrahedron	×4		0.0207	0.0213	0.0214	0.0219	0.0225	0.0229	0.0232
Voids		18.98	111.512	106.818	103.913	100.499	96.502	93.222	90.342

$^{(1)}$-$^{(5)}$ Number labels the different Ca-O bond by their lengths. $^{(1), (5)}$ represent the longest and shortest Ca-O bond, respectively. [ ] Number of bond lengths/angles used to compute the average.

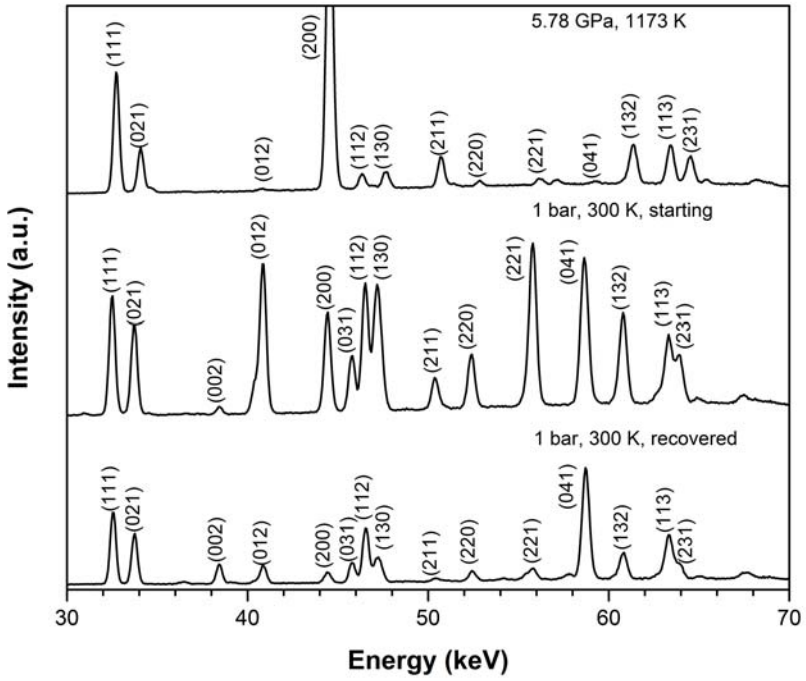

458
459 **Fig. 1.**
460
461
462

463

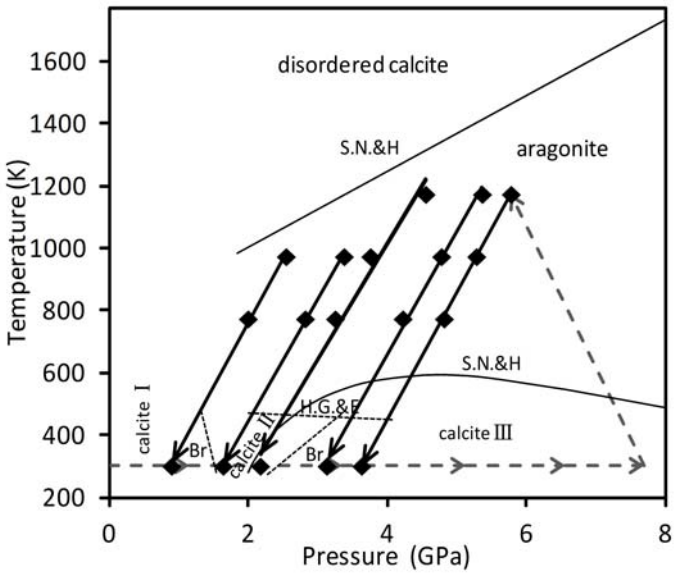

464
465 **Fig. 2.**

466

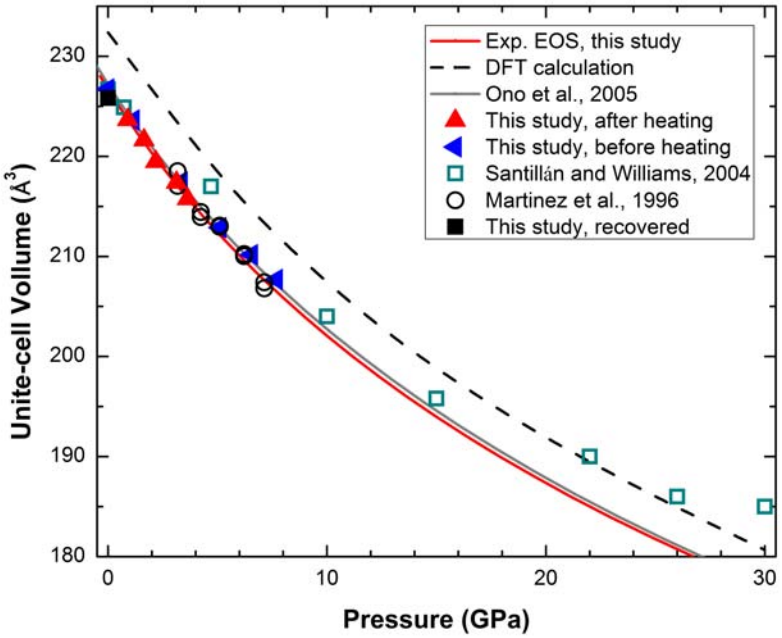

467
468 **Fig. 3.**

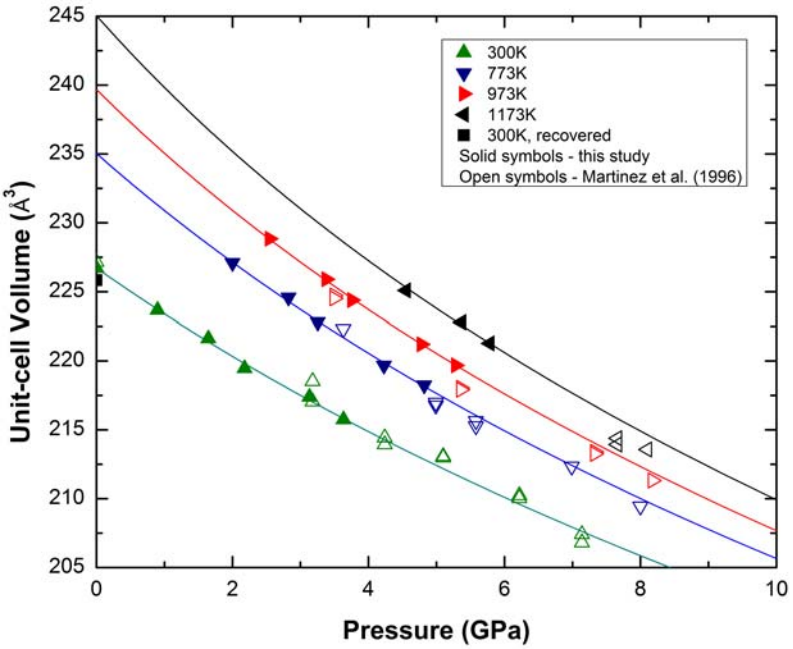

469
470 **Fig. 4.**

471

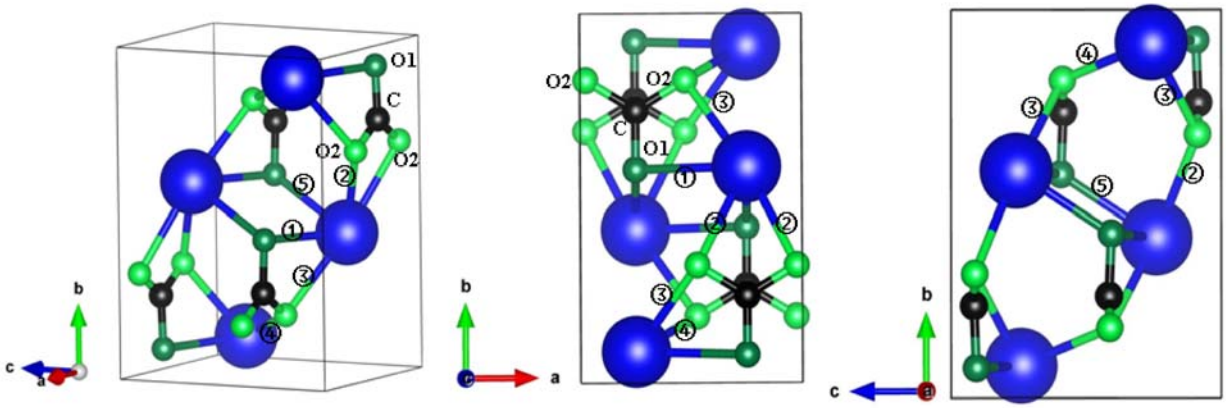
O1
C
O2
O2
O2
C
O1
b
c
a
b
a
b
c

Fig. 5.

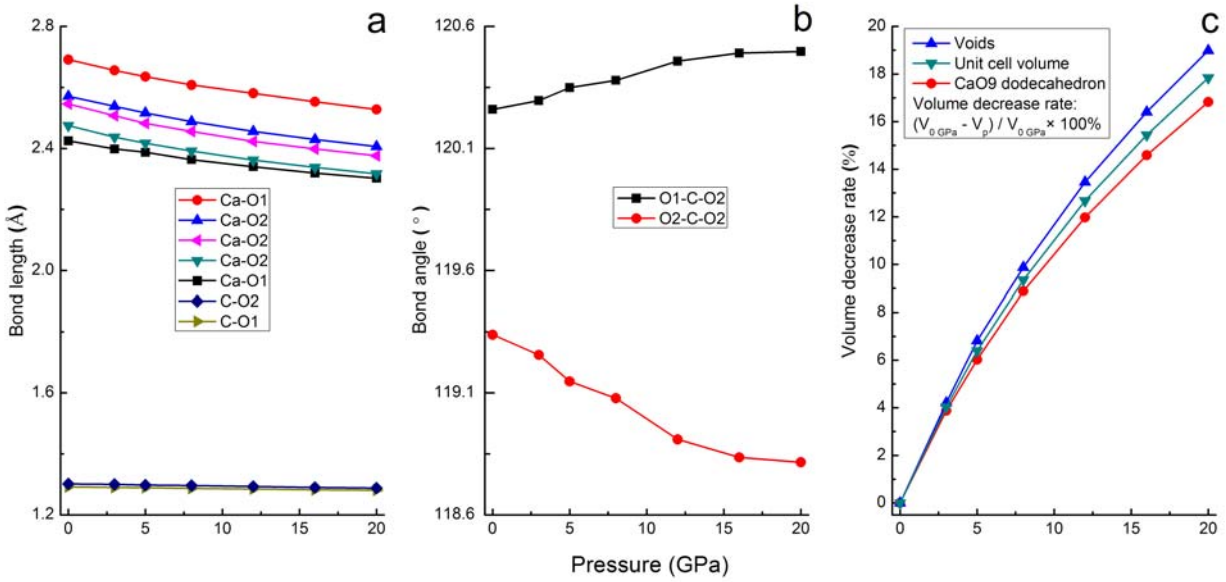
a
Bond length (Å)
Ca-O1
Ca-O2
Ca-O2
Ca-O2
Ca-O1
C-O2
C-O1
b
Bond angle (°)
O1-C-O2
O2-C-O2
Pressure (GPa)
c
Volume decrease rate (%)
Voids
Unit cell volume
CaO9 dodecahedron
Volume decrease rate:
(V0 GPa - Vp) / V0 GPa × 100%

Fig. 6.

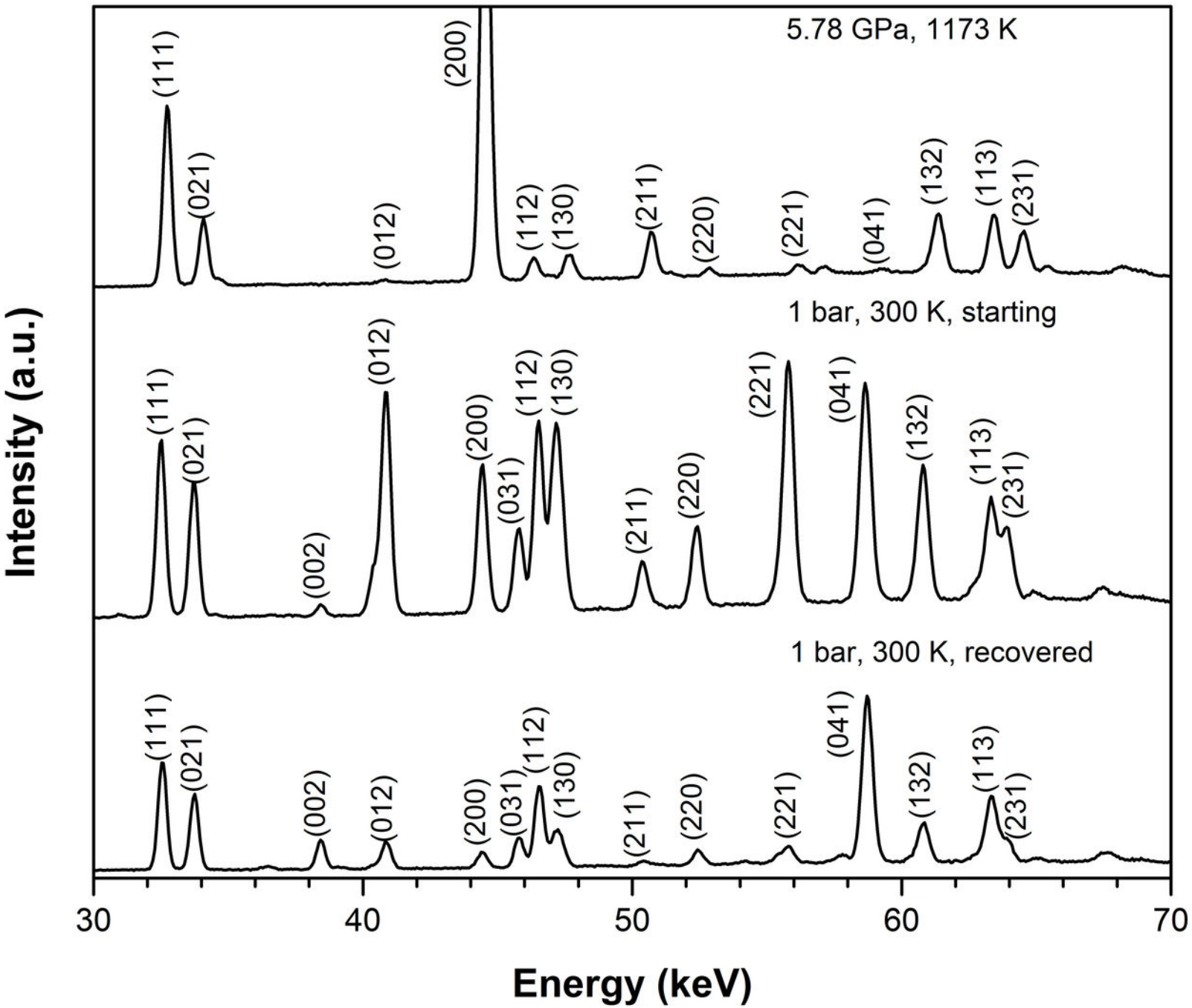
5.78 GPa, 1173 K
(111)
(021)
(012)
(200)
(112)
(130)
(211)
(220)
(221)
(041)
(132)
(113)
(231)
1 bar, 300 K, starting
(111)
(021)
(002)
(012)
(200)
(031)
(112)
(130)
(211)
(220)
(221)
(041)
(132)
(113)
(231)
1 bar, 300 K, recovered
(111)
(021)
(002)
(012)
(200)
(031)
(112)
(130)
(211)
(220)
(221)
(041)
(132)
(113)
(231)
Intensity (a.u.)
30
40
50
60
70
Energy (keV)

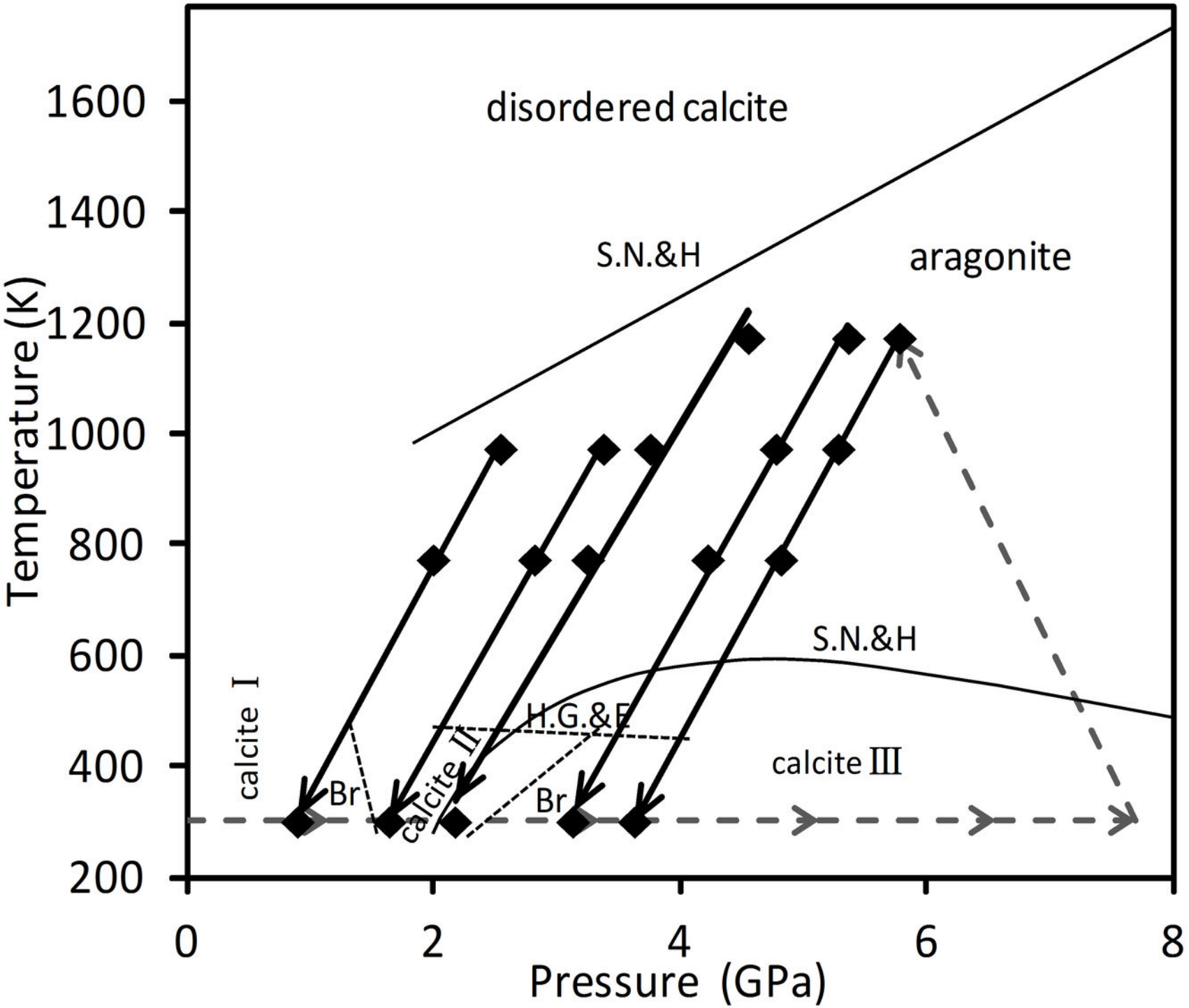
1600
1400
1200
1000
800
600
400
200
Temperature (K)
0
2
4
6
8
Pressure (GPa)
disordered calcite
S.N.&H
aragonite
S.N.&H
H.G.&F
calcite I
calcite II
calcite III
Br
Br

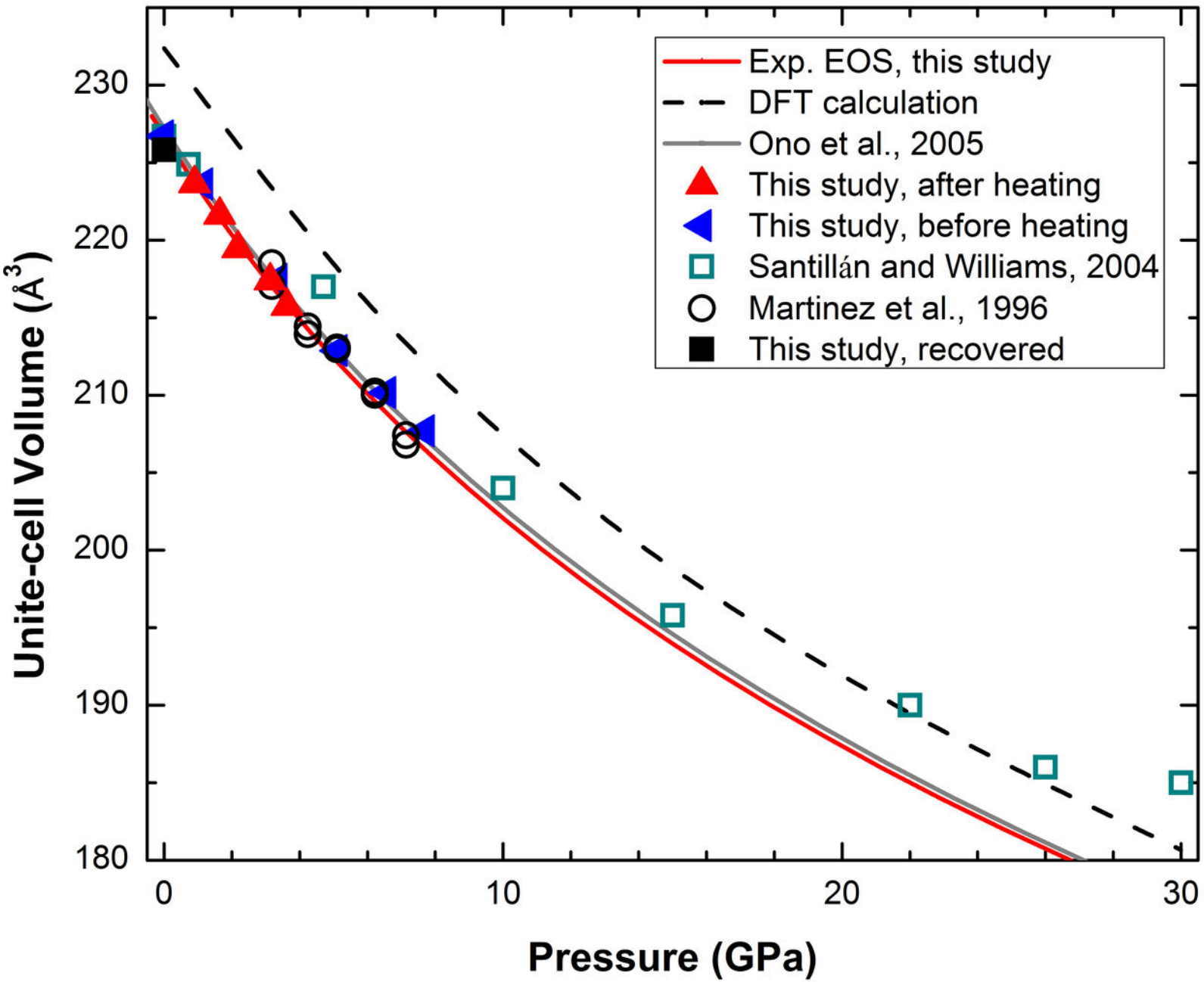
Exp. EOS, this study
DFT calculation
Ono et al., 2005
This study, after heating
This study, before heating
Santillán and Williams, 2004
Martinez et al., 1996
This study, recovered
Unite-cell Vollume (Å^3)
230
220
210
200
190
180
0
10
20
30
Pressure (GPa)

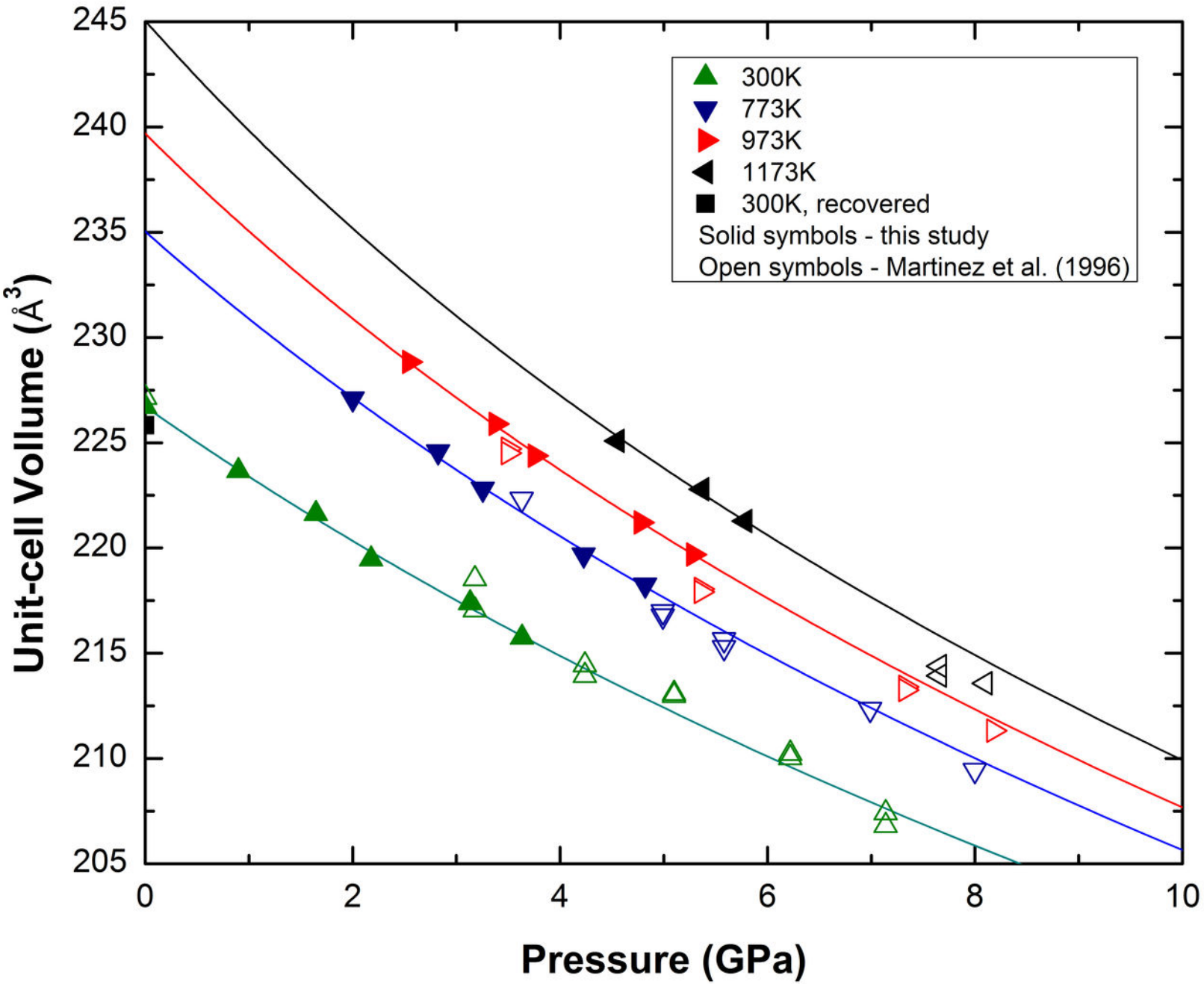
300K
773K
973K
1173K
300K, recovered
Solid symbols - this study
Open symbols - Martinez et al. (1996)
Unit-cell Vollume (Å^3)
Pressure (GPa)
245
240
235
230
225
220
215
210
205
0
2
4
6
8
10

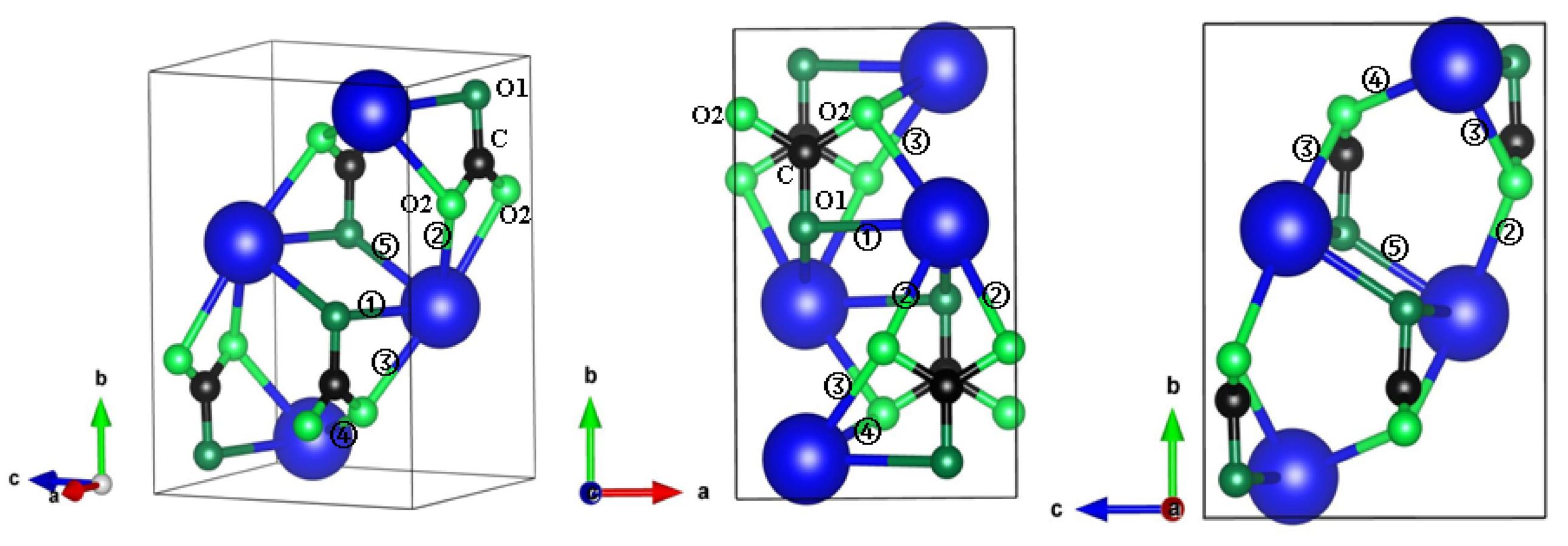
O1
C
O2
O2
5
2
1
3
4
b
c
a
O2
O2
C
O1
3
1
2
2
3
4
b
c
a
4
3
3
5
2
b
c
a

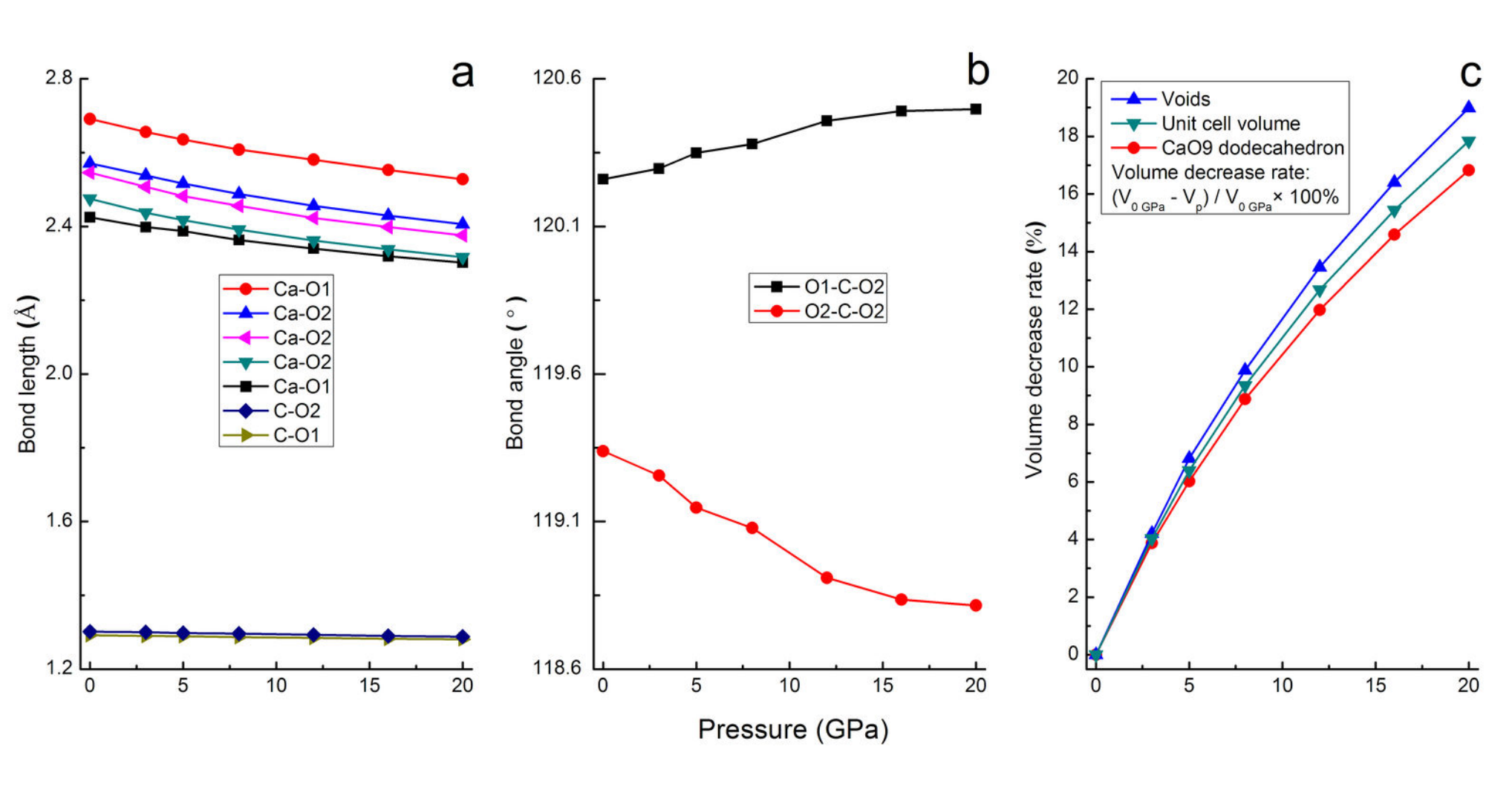
a
Bond length (Å)
2.8
2.4
2.0
1.6
1.2
0
5
10
15
20
Ca-O1
Ca-O2
Ca-O2
Ca-O2
Ca-O1
C-O2
C-O1
b
Bond angle (°)
120.6
120.1
119.6
119.1
118.6
O1-C-O2
O2-C-O2
Pressure (GPa)
c
Volume decrease rate (%)
Voids
Unit cell volume
CaO9 dodecahedron
Volume decrease rate:
(V0 GPa - Vp) / V0 GPa × 100%